

Hierarchical Lyotropic Liquid Crystalline Behaviors of Supramolecular Polymers Influenced by Alkyl Chain Branching

Cong Wang,² Fei Xie,¹ Hua Zhong,² Feng Wang^{2*} and Ningdong Huang,^{1,3*}

¹ National Synchrotron Radiation Lab, University of Science and Technology of China, Hefei, Anhui 230026, P. R. China. E-mail: ndhuang@ustc.edu.cn

² CAS Key Laboratory of Soft Matter Chemistry, Department of Polymer Science and Engineering, University of Science and Technology of China, Hefei, Anhui 230026, P. R. China. E-mail: drfwang@ustc.edu.cn

³ School of Nuclear Science and Technology, University of Science and Technology of China, Hefei, Anhui 230026, P. R. China.

Supporting Information

1. *Materials and methods*
2. *Thermotropic liquid crystalline behaviors of 1–2*
3. *¹H NMR and FTIR measurements of 1–2*
4. *Lyotropic liquid crystalline behaviors of 1–2*
5. *2D electron density reconstruction of 2*
6. *Synthetic routes to 1–2*

1. Materials and methods

N-(3-dimethylaminopropyl)-*N*'-ethylcarbodiimide hydrochloride (EDC), 4-dimethylamino pyridine (DMAP), adipic acid, *N*-boc-ethylenediamine and trifluoroacetic acid are reagent grade and used as received. All solvents are commercially available and were employed as received without further purification. Compound **5** was synthesized according to a previously reported procedure.^{S1}

¹H NMR spectra were collected on a Varian Unity INOVA-400 spectrometer with TMS as the internal standard in deuteriochloroform. ¹³C NMR spectra were recorded on a Varian Unity INOVA-400 spectrometer at 100 MHz. UV/Vis spectra were recorded on a UV-1800 Shimadzu spectrometer analyzed with an Origin (v9.0). Circular dichroism (CD) measurements were performed on a Jasco J-1500 circular dichroism spectrometer, equipped with a PFD-425S/15 Peltier-type temperature controller. All the temperature dependent CD measurements were conducted at a temperature slope of 1 K min⁻¹. Transmission electron microscopy (TEM) experiments were performed on a Tecnai G2 Spirit BioTWIN electron microscope (acceleration voltage: 120 kV). The sample were dropped onto carbon-coated copper grids and freely dried in ambient conditions. Scanning electron microscopy (SEM) images were obtained on a SU8220 (HITACHI, Japan) with an acceleration voltage of 2 kV. Polarizing optical microscopy (POM) experiments were performed an Olympus (Japan) BX-51-P microscope system with a polarizing attachment and a full-wave retardation plate ($\lambda = 530$ nm). Synchrotron radiation Small Angle X-Ray Scattering (SAXS) measurements were performed at beamline 16B1 in the Shanghai Synchrotron Radiation Facility (SSRF). The X-ray photon wavelength of 0.124 nm was used with a Pilatus detector (1475×1679 pixel dimension and 172 μm^2 pixel size). A sample-to-detector distances of 1970 mm was employed to collect 2D SAXS patterns which achieved by using the position of the diffraction peaks of a standard silver behenate sample. The scattering patterns analyzed with Fit2D software from the European Synchrotron Radiation Facility based on the scattering vector $q = (4\pi/\lambda) \times \sin(\theta/2)$ where θ is the scattering angle and λ is X-ray wavelength. Electron density reconstruction maps were obtained by utilizing the matlab 16 software package.

Determination of the thermodynamics for supramolecular polymerization process: Normalized CD melting curves of **2** were fitted with the one-component equilibrium model^{S2}

to obtain the thermodynamic parameters for the supramolecular polymerization process. The dynamic equilibrium between free monomers and the supramolecular polymer, as well as the growth of the corresponding polymer, are taken into account in this model. The elongation and nucleation reactions are described by the constants K_1 and K_2 depending on the temperature, and the parameter σ represent the degree of cooperativity. The thermodynamic parameters can be determined by following the equations:

$$K_1 = e^{-(\Delta H^0 - T\Delta S^0)/(RT)} \quad \text{Eq. S1}$$

$$K_2 = K_1 e^{(\Delta H_{mm}^0)/(RT)} \quad \text{Eq. S2}$$

$$\sigma = \frac{\tilde{K}_1}{K_1} = \frac{\tilde{K}_2}{K_2} = e^{(\Delta H_{\text{nucl}}^0)/(RT)} \quad \text{Eq. S3}$$

In these equations, K_1 and K_2 denote equilibrium constants for the elongation and nucleation regime. ΔH^0 and ΔH_{nucl}^0 stand for the elongation enthalpy and nucleation penalty, respectively. R represents the universal gas constant.

2. Thermotropic liquid crystalline behaviors of 1–2

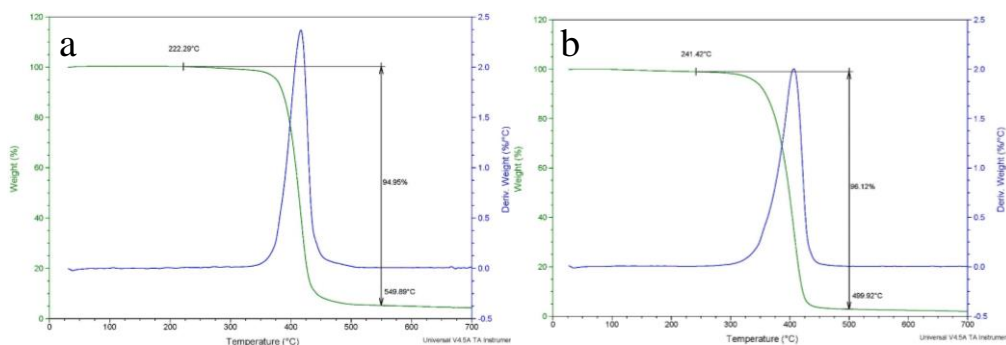


Figure S1. Thermal gravimetric measurement for compounds a) **1** and b) **2** under a nitrogen atmosphere. **1** and **2** show a comparably good thermal stability under a nitrogen atmosphere.

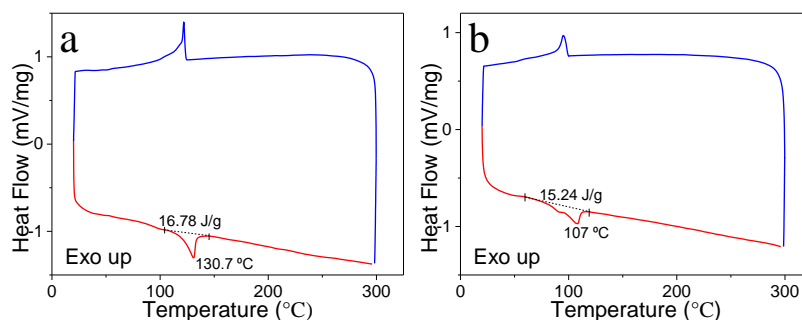


Figure S2. DSC curves under the nitrogen atmosphere of compounds a) **1** and b) **2** upon second heating (red lines) and first cooling (blue lines), where the dashed lines were used as the baselines to calculate the phase transition enthalpy. The thermal transition temperature of compound **2** (107.0 °C) was 23.7 °C lower than that of **1**. The lower melting temperature indicates less ordered LC structure endowed by the branched alkyl chains on **2**.

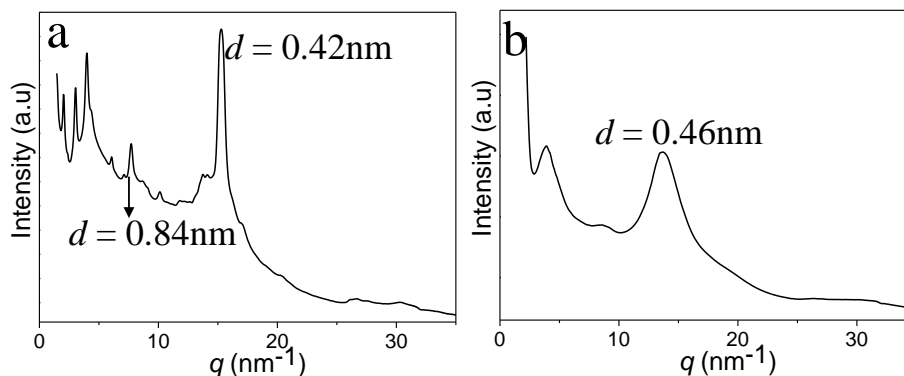


Figure S3. WAXS curves of a) **1** and b) **2** in solid state. Compound **1** showed two sharp diffractions peaks in the wide-angle region, with the d -spacing of 0.42 nm and 0.84 nm,

respectively. They correspond to the *d*-spacings of hydrogen bonds distances between the amide units. In comparison, **2** showed a broad peak with the *d*-spacing of 0.46 nm, typical for intermolecular stack between the peripheral tails. Thereby the phenomena indicate less ordered packing of **2** than **1** in the solid state.

3. ^1H NMR and FTIR measurements of **1**–**2**

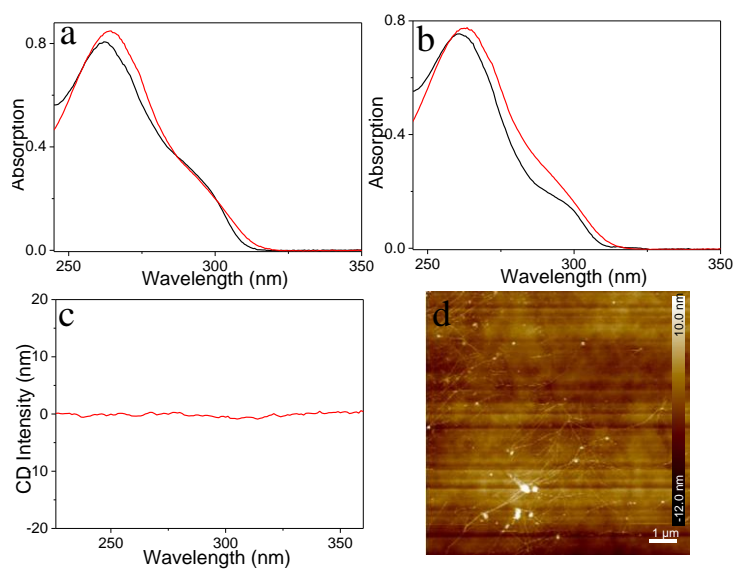


Figure S4. UV-Vis absorption spectra of a) **1** and b) **2** in decane (4.0×10^{-5} M at 293K and 343K); c) CD spectra of **1** ($c = 4.0 \times 10^{-5}$ M, in decane) at 293 K; d) AFM image of **1**. No Cotton effects was observed for **1** because of the absence of stereo centers in its structure, Meanwhile, AFM confirmed the formation of fibrillar morphology with tens of micrometers in length, supporting the formation of supramolecular polymers **1**.

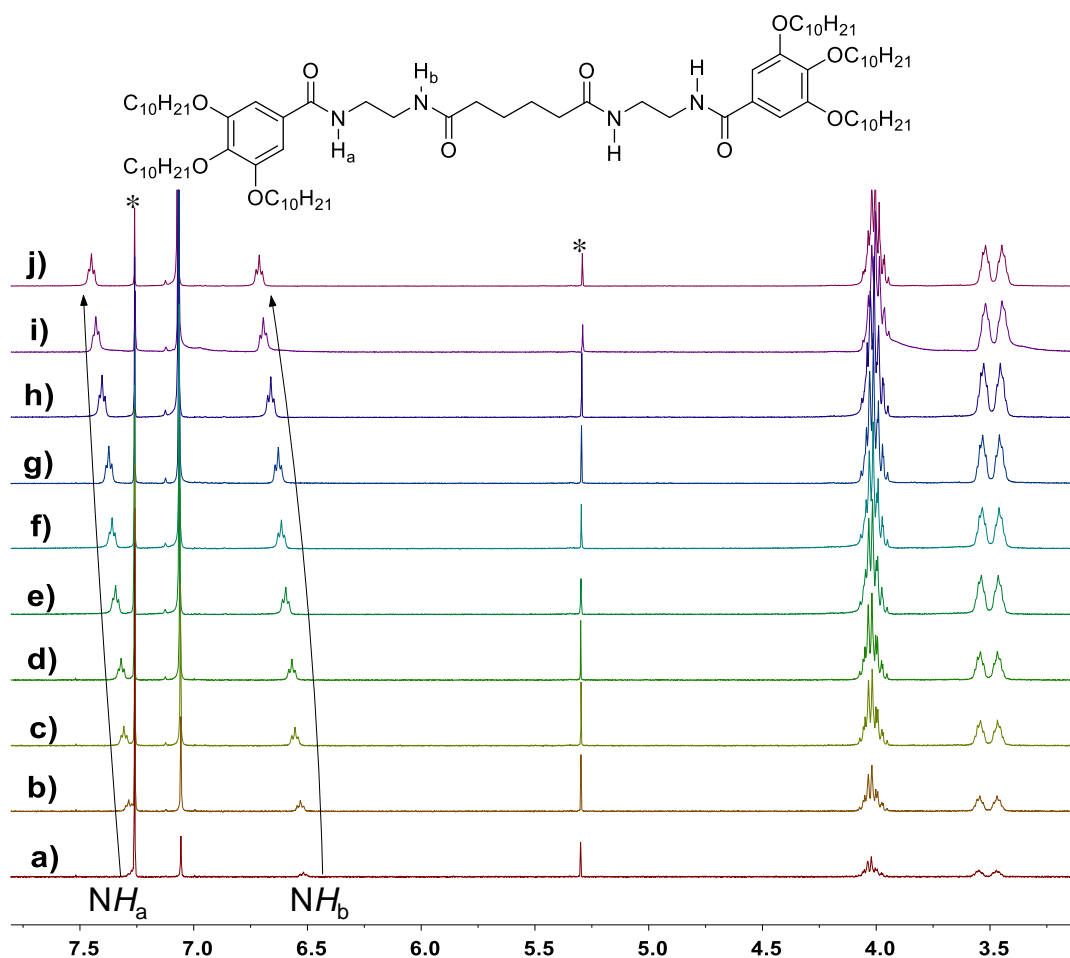


Figure S5. Concentration-dependent ^1H NMR spectra (400 MHz, CDCl_3 , 298 K) of **2**: a) 1.25 mM; b) 2.50 mM; c) 5.00 mM; d) 7.50 mM; e) 10.0 mM; f) 12.5 mM; g) 15.0 mM; h) 20.0 mM; i) 25.0 mM; j) 30.0 mM. The asterisks represent the solvent peaks. The arrows show the shifting of NH protons. Upon increasing the monomer concentration of **2** from 1.25 mM to 30.0 mM in *d*-chloroform, both amides NH resonances exhibit significant downfield shifts (NH_a : from 7.27 to 7.45 ppm, NH_b : from 6.52 to 6.71 ppm). It is evident that intermolecular hydrogen bonds exist in the supramolecular assembly process.

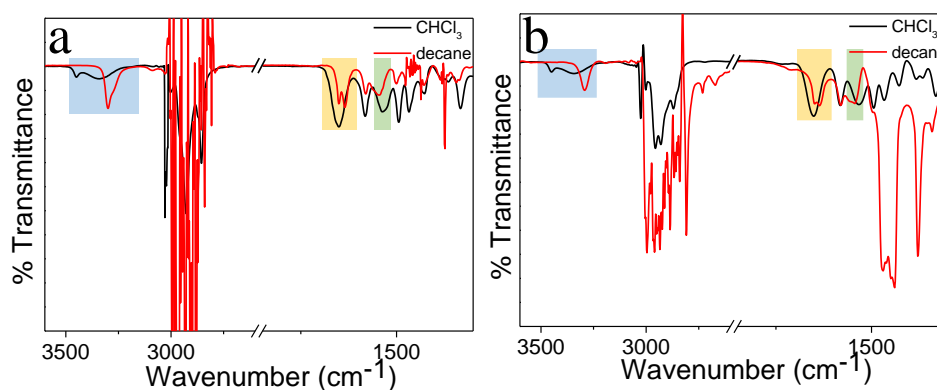


Figure S6. Fourier transform IR spectroscopy of a) **1** and b) **2** (1.0×10^{-3} M) in CHCl_3 and decane solution, respectively. Blue: N–H stretch bands; yellow: CO stretch bands; green: amide II bands. Upon switching the solvent to apolar decane, the broad N–H stretching

vibration and the H-bonded C=O stretching move to short wavenumber (N–H stretching: from 3350 to 3302 cm^{-1} for **1** and from 3350 to 3293 cm^{-1} for **2**; C=O stretching: from 1650 to 1635 cm^{-1} for **1** and from 1652 to 1636 cm^{-1} for **2**, respectively). It is evident that intermolecular hydrogen bonds form in the supramolecular polymerization process.

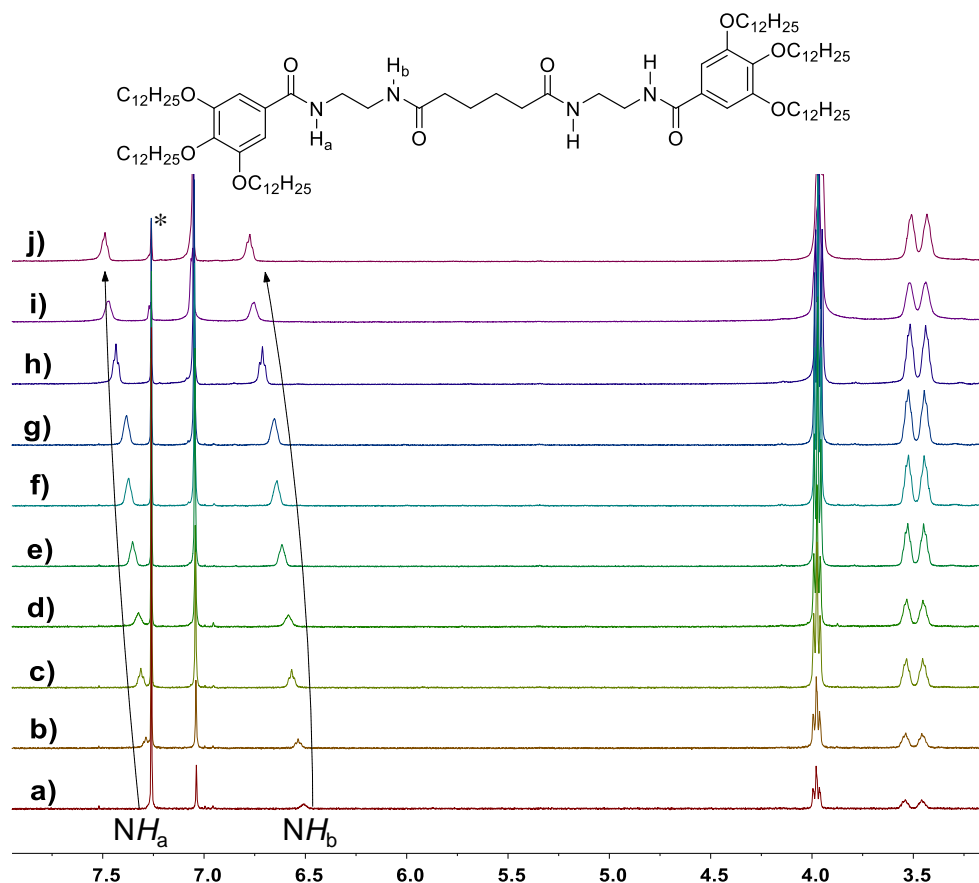


Figure S7. Concentration-dependent ^1H NMR spectra (400 MHz, CDCl_3 , 298 K) of monomer **1**: a) 1.25 mM; b) 2.50 mM; c) 5.00 mM; d) 7.50 mM; e) 10.00 mM; f) 12.50 mM; g) 15.00 mM; h) 20.00 mM; i) 25.00 mM; j) 30.00 mM. The asterisk represents the solvent peak. The arrows show the shifting of NH protons. Upon increasing the monomer concentration of **1** from 1.25 mM to 30.0 mM in *d*-chloroform, both amides NH resonances exhibit significant downfield shifts (NH_a : from 7.28 to 7.49 ppm, NH_b : from 6.52 to 6.77 ppm).

4. Lyotropic liquid-crystalline behavior of 1–2

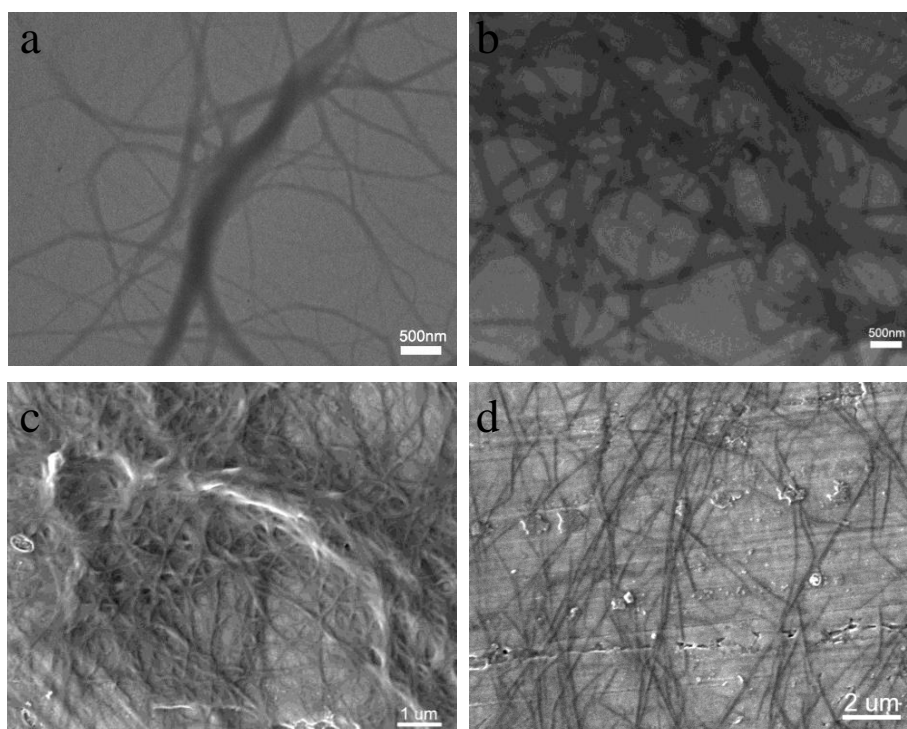


Figure S8. TEM images of a) **1** and b) **2** and SEM images of c) **1** and d) **2** ($c = 1.00 \times 10^{-4}$ M). Both TEM and SEM measurements of **1–2** show fibrous morphology extending hundreds micrometers long and diameter varies from dozens to hundreds of nanometers.

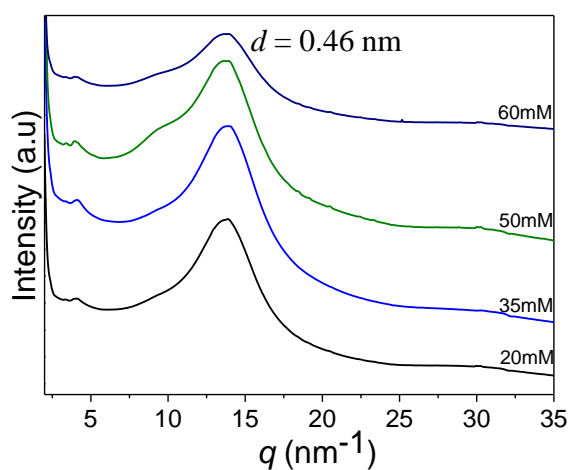


Figure S9. WAXS curves of **2** in decane at different concentration. The WAXS of **2** features a main broad peak around 13.7 nm^{-1} which is characteristic of intermolecular organization of the peripheral alkyl chains.

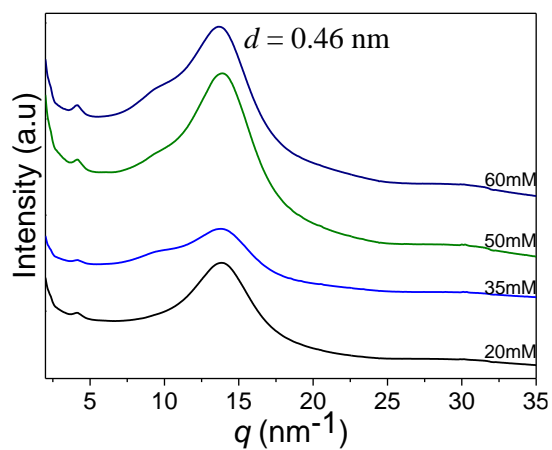


Figure S10. WAXS curves of **1** in decane at different concentration. The WAXS of **1** features a main broad peak around 13.7 nm^{-1} which is characteristic of intermolecular organization of the peripheral alkyl chains.

5. 2D electron density reconstruction of 2

In order to reconstruct the electron density maps of the LC solution the diffraction intensities were measured for all Bragg peaks. The different scattering powers of the solvent and the solute are reflected in the diffraction intensities, which are related by Fourier transformation to the electron density distribution $E(x,y)$ in the unit cell. For 2D structures:

$$E(x, y) = \sum_{h,k} F(hk) \exp[i2\pi(hx + ky)] = \sum_{h,k} \sqrt{I(hk)} \exp[i2\pi(hx + ky) + \phi] \quad \text{Eq. S4}$$

where $I(hk) = |F(hk)|^2$ is the intensity of the diffraction peak.

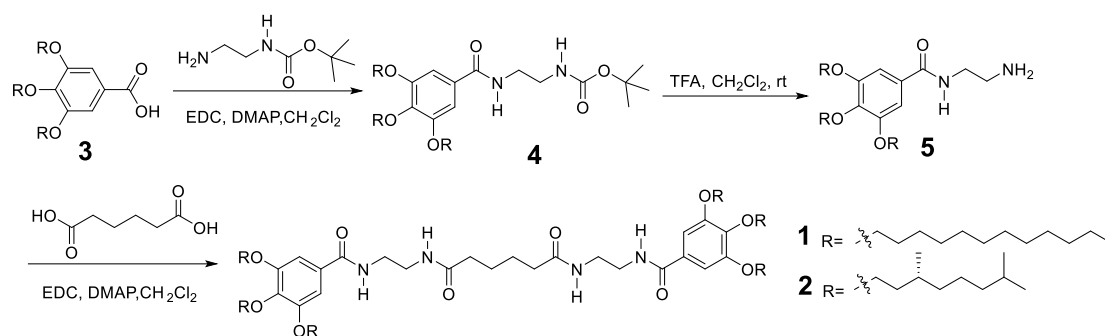
In general, the structure factor $F(hk)$ is a complex number, so the phase angle ϕ could range from 0 to 2π . The phase angle ϕ cannot be determined directly from diffraction experiments. However, for centro-symmetric structures such as the hexagonal columnar, plane group $p6mm$, the problem is simplified by the fact that $F(hk)$ is a real number and the phase angle ϕ can only take up the values 0 or π *i.e.* the scattering amplitudes $F(hk)$ are equal to $|F(hk)|$ with either a positive or a negative sign. For LC systems, where the number of observed reflections is relatively limited, this allows one to examine all possible phase combinations, and the choice of a combination can be made on the merit of each reconstructed ED map. Even so, since the number of possible maps corresponding to a diffractogram with m reflections is 2^m , the task could still appear somewhat daunting. Fortunately weak reflections could be ignored as they will have little effect on the gross features of $E(x,y)$.

In the present case the situation is particularly favourable since with changing concentration the structure is expected to change slowly, meaning that the amplitude $F(hk)$ of each reflection will also change slowly. Thus the zero crossing and the change of sign of $F(hk)$ could be identified by plotting $F(hk)$ against c . In this way the signs of $F(hk)$ and the candidate maps are not chosen in isolation, but are compared to those at lower and higher concentration, bearing in mind what effects a change in concentration could realistically be expected to have on the structure.

Table S1. q -values (nm^{-1}) of the observed Bragg reflections for different solution concentrations. q -values of observed reflections divided by n , where $n = h^2+k^2+hk$. The resulting lattice parameter $a=4\pi/\sqrt{3}/q_{100}$, based on the average of all q/n values, is given in the last column.

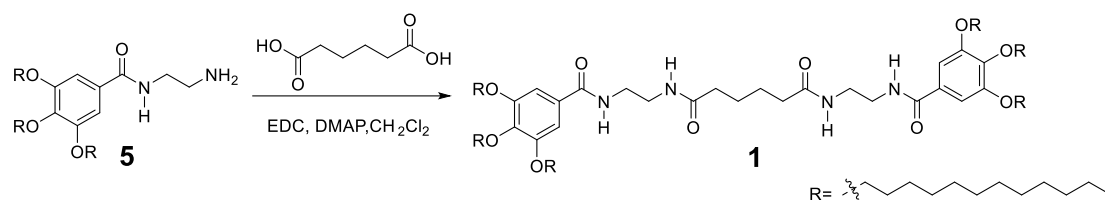
hkl	Q			$q_{100}=q/N$			$\langle q_{100} \rangle$	$a(\text{\AA})$
	100	110	200	100	110	200		
N	1	3	4	1	3	4		
5mM	1.92	–	–	–	–	–	–	–
10mM	1.90	3.42	3.87	1.90	1.97	1.94	1.94	37.4
15mM	1.91	3.41	3.87	1.91	1.97	1.94	1.94	37.4
20mM	1.91	3.42	3.89	1.91	1.97	1.95	1.94	37.4
30mM	1.90	3.41	3.89	1.90	1.97	1.95	1.94	37.4
40mM	1.92	3.39	3.90	1.92	1.96	1.95	1.94	37.4
50mM	1.93	3.39	3.89	1.93	1.96	1.95	1.95	37.2
60mM	1.92	3.41	3.89	1.92	1.97	1.95	1.95	37.2

6. Synthetic routes to 1–2



Scheme S1. Synthetic routes to the targeted compounds 1–2.

6.1. Synthesis of compound 1



Adipic acid (37.0 mg, 0.25 mmol), EDC (107.4 mg, 0.56 mmol), and 4-dimethylamino pyridine (68.0 mg, 0.56 mmol) were dissolved in 50 ml of CH_2Cl_2 under nitrogen and stirred for 15 min with ice bath. Compounds **5** (400 mg, 0.56 mmol) in 10 ml CH_2Cl_2 were added dropwise to the reaction solution and continued to stir at room temperature for 12 hours. After the reaction was completed, the reaction solution was washed with HCl (1M), NaHCO_3 (1M) and water. After drying with anhydrous Na_2SO_4 , the solvent was evaporated with a rotary evaporator. The residue was purified by flash column chromatography (silica, with Methanol/ dichloromethane, 4/96, v/v, as the eluent) to afford **1** as light yellow solid (290mg, 75%). ^1H NMR (400 MHz, CDCl_3) δ = 7.46 (t, J = 5.2 Hz, 1H), 7.05 (s, 4H), 6.74 (t, J = 5.6 Hz, 2H), 3.96 (m, 12H), 3.52 (m, 4H), 3.43 (m, 4H), 2.08 (d, J = 5.5 Hz, 4H), 1.75 (m, 12H), 1.55 – 1.15 (m, 112H), 0.87 (t, J = 6.7 Hz, 18H). ^{13}C NMR (101 MHz, CDCl_3) δ (ppm): 174.4, 168.1, 153, 141.1, 128.8, 105.8, 73.5, 69.2, 41.3, 39.5, 36.0, 30.3, 29.7, 29.6, 29.4, 29.3, 26.1, 25.0, 22.7, 14.1. MALDI-TOF-MS m/z : $[\text{M} + \text{Na}]^+$, $\text{C}_{96}\text{H}_{174}\text{N}_4\text{NaO}_{10}$, calculated 1566.3122; found 1566.6163.

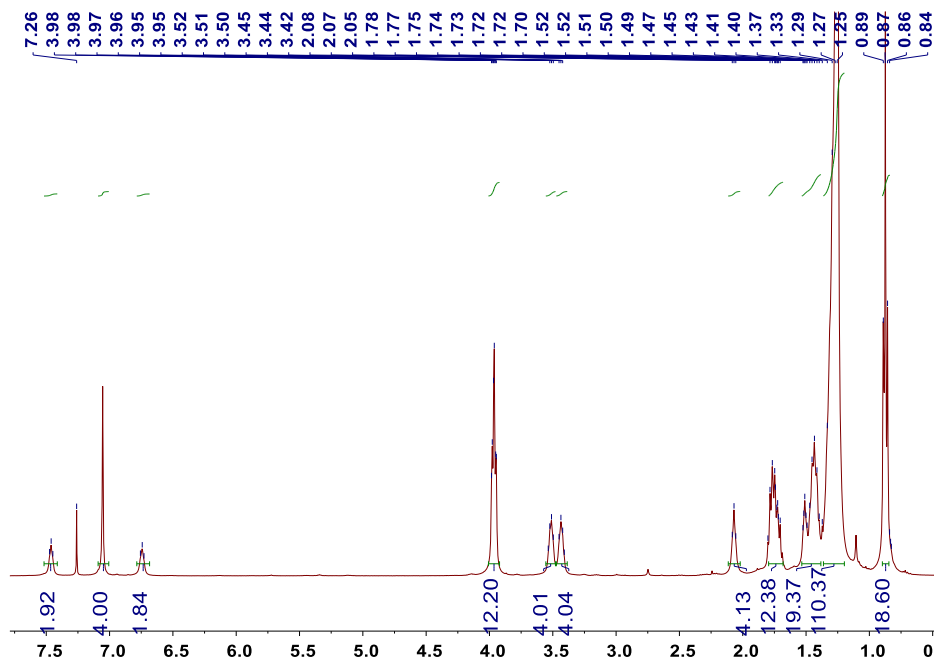


Figure S11. ^1H NMR spectrum (400 MHz, CDCl_3 , room temperature) of compound **1**.

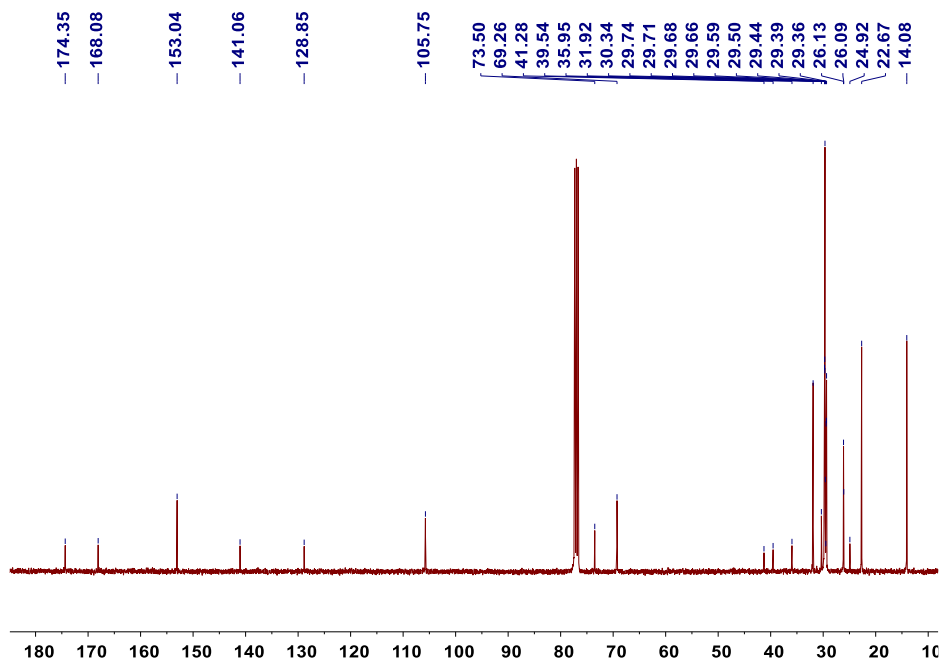


Figure S12. ^{13}C NMR spectrum (100 MHz, CDCl_3 , room temperature) of **1**.

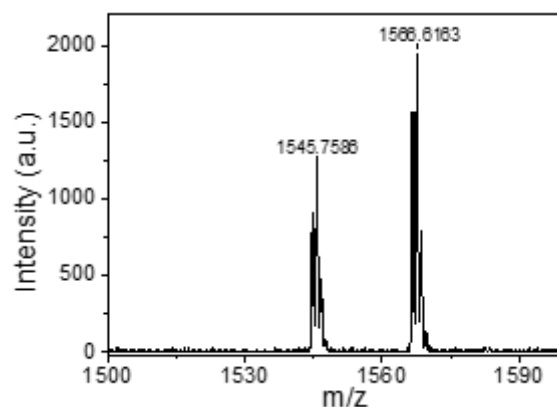
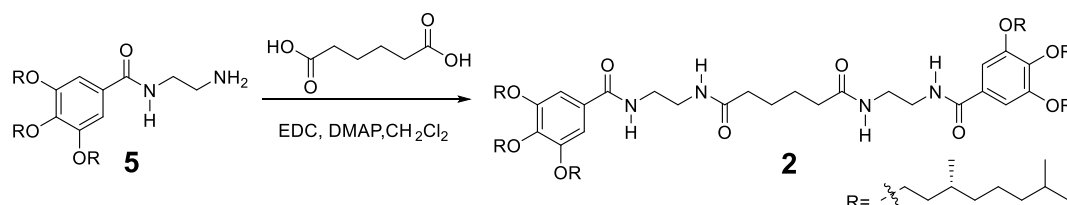


Figure S13. MALDI-TOF mass spectrum of **1**

6.2. Synthesis of compound **2**



Adipic acid (41.9 mg, 0.29 mmol), EDC (122.3 mg, 0.63 mmol), and 4-dimethylamino pyridine (76.9 mg, 0.63 mmol) were dissolved in 50 ml of CH_2Cl_2 under nitrogen and stirred for 15 min with ice bath. Compounds **5** (400 mg, 0.63 mmol) in 10 ml CH_2Cl_2 were added dropwise to the reaction solution and continued to stir at room temperature for 12 hours. After the reaction was complete, the reaction solution was washed with HCl (1M), NaHCO_3 (1M), and water. After drying with anhydrous Na_2SO_4 , the solvent was evaporated with a rotary evaporator. The residue was purified by flash column chromatography (silica, with Methanol/ dichloromethane, 4/96, v/v, as the eluent) to afford **2** as light yellow solid (284mg, 70%). ^1H NMR (400 MHz, CDCl_3) δ = 7.40 (t, J = 5.0 Hz, 2H), 7.07 (s, 4H), 6.66 (t, J = 5.7 Hz, 2H), 4.02 (m, 12H), 3.53 (m, 4H), 3.45 (m, 4H), 2.07 (d, J = 6.1 Hz, 4H), 1.90 – 1.76 (m, 8H), 1.73 – 1.44 (m, 20H), 1.38 – 1.07 (m, 36H), 0.91 (dd, J = 6.6, 1.4 Hz, 18H), 0.86 (d, J = 6.6 Hz, 36H). ^{13}C NMR (101 MHz, CDCl_3) δ (ppm): 174.4, 168.1, 153.0, 140.9, 128.8, 105.6, 71.7, 67.5, 41.3, 39.5, 37.4, 36.4, 36.0, 29.7, 28.0, 24.9, 24.7, 22.6, 19.5. MALDI-TOF-MS m/z : $[\text{M} + \text{Na}]^+$, $\text{C}_{84}\text{H}_{150}\text{N}_4\text{NaO}_{10}$, calculated 1398.1250; found 1398.1244.

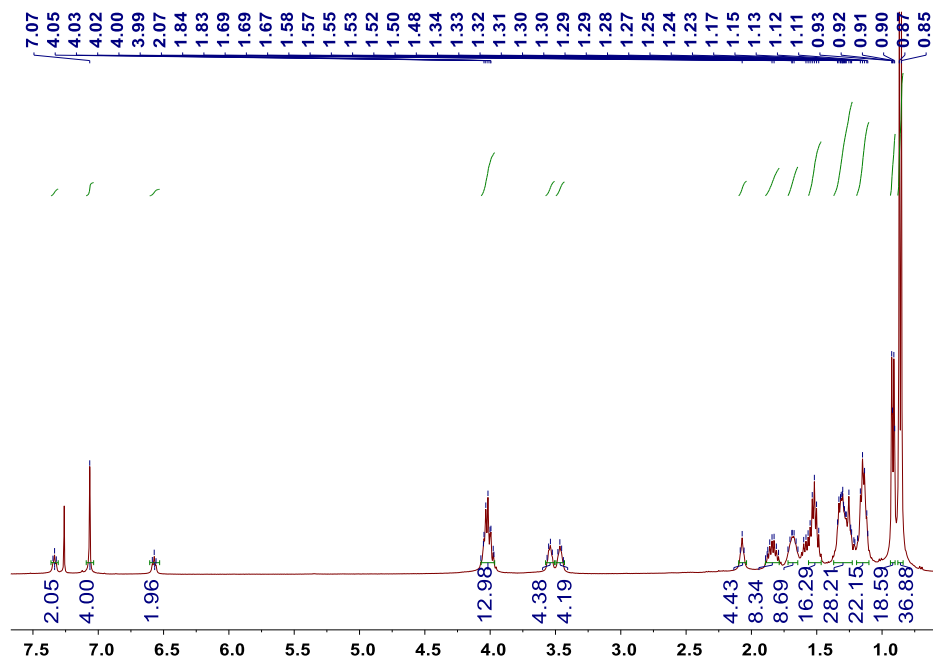


Figure S14. ^1H NMR spectrum (400 MHz, CDCl_3 , room temperature) of compound 2.

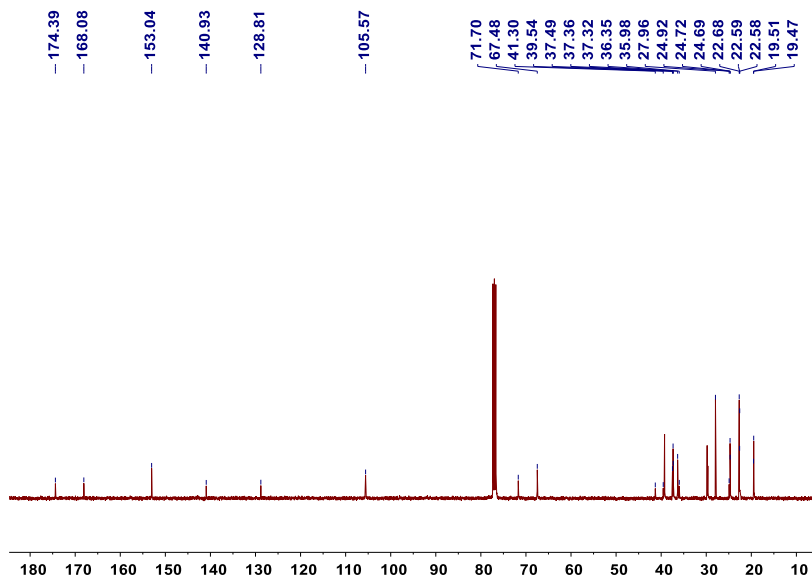


Figure S15. ^{13}C NMR spectrum (100 MHz, CDCl_3 , room temperature) of 2.

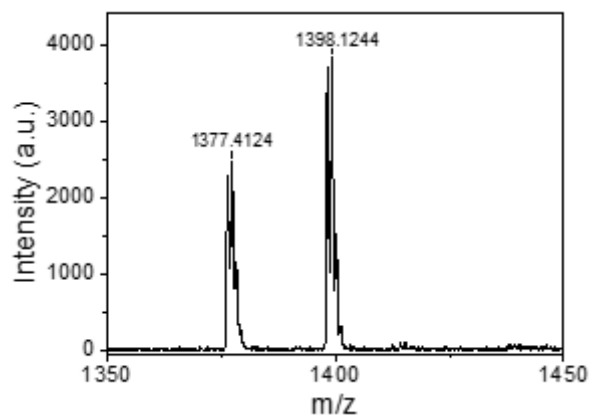


Figure S16. MALDI-TOF mass spectrum of **2**

REFERENCES:

- S1. F. Aparicio and L. Sánchez, *Chem. Eur. J.*, **2013**, *19*, 10482.
S2. H. M. M Eikelder, A. J. Markvoort, T. F. A. Greef and P. A. J. Hilbers, *J. Phys. Chem. B*, **2012**, *116*, 5291.